A Dynamic Interface Algorithm in Immersed-Finite-Element Particle-in-Cell Method

Huijun Cao[1,2,*], Yuxi Yu[2], Zhihao Zhang[2]

1. School of Mechanical and Automation Engineering, Xiamen City University, Xiamen 361005, China

2. Fujian Key Laboratory of Advanced Materials, College of Materials, Xiamen University, Xiamen 361005, China

Abstract: The evolution of wall surface in all engineering plasma problems is unavoidable. An improved approach with dynamic boundary to modeling plasma-wall interactions which is based on the immersed finite element particle-in-cell (IFE-PIC) algorithm is presented. The Huygens wavelet method which shows great superiority to handle surface evolution problems is inducted into the common IFE-PIC method to realize the dynamic changes of boundary surfaces. Numerical example is provided to demonstrate features of this dynamic boundary method. Additionally, a typical engineering surface evolution problem, the erosion of ion thruster accelerator grid, is simulated to show the practicability and accuracy of this method.

Keywords: IFE-PIC; Dynamic boundary; Huygens wavelet method; Plasma-wall interactions

1 Introduction

In practical engineering plasma-wall interactions, the ion sputtering which can remove the surface layers on a atomic scale is unavoidable[1-4]. Thus, the wall surfaces are constantly and gradually evolving. A typical example is the grid erosion of the electron propulsion [5-8]. Ion thrusters which use accelerated ion beam to create thrust have been widely applied in deep space mission[9,10]. The biggest limitation of promoting longevity of ion thruster is the erosion of its accelerator grid[11,12]. The ions obtain high kinetic energy when pass through the extraction system and unavoidable collide with the accelerate grid, eroding it and compromising the engine's longevity. It not only reduces efficiency, but also limits the longevity of the thruster[5,6,8].

Although the surface evolution does not change the mechanism and property of the plasma, it affects the trajectories of the particles and the distribution of the electric field. Many simulation models are introduced to describe this kind of plasma problems and most of the mare based on the PIC method[5-7]. This method treats the plasma as particles[13], thus it can have a more reality result of the particle movements and incident parameters. The common unstructured mesh which imports a lot of difficul-

* Corresponding author (huijun@xmcu.cn)

ties in locating the particles is unsuitable for modeling the plasma problems. Moreover, it is even unsuitable for handling evolving surface because it needs a new mesh after every change of the surface morphology. Thus, most PIC simulations are based on the structured Cartesian mesh. But this mesh requirement limits the PIC method to simulating plasma problems with regular or simplified configurations. For practical engineering applications, a PIC code needs to be more sophisticated to model complex geometric and field effects associated with the device surface.

Recently, the immersed finite element (IFE) algorithm[14,15] which provides a new approach to solve interface problems with grid meshes independent on the interface, is developed and well established for interface problems. T. Lin etal.[14] validate and extend this algorithm in mathematics, details can be seen in[14] and the references therein. The advantages of this algorithm are that the IFE can create a structured Cartesian mesh and it is independent on the material interfaces. It shows great superiority for electric or electromagnetic field solution in large-scale PIC simulations of problems involving complex boundary conditions. Many researchers do a lot of work to incorporate the IFE algorithm into the well-developed PIC code and then introduce the IFE-PIC algorithm. In this algorithm, the IFE formulation develops the mesh and solves the electric or electromagnetic field and the standard PIC handles the movements of all particles. Kafafy, Wang and Cao et.al[16-20] even introduce this IFE-PIC method to studying the plasma problems about ion-optical thruster. On the other wise, the erosion phenomenon is also studied in many researches[6,21-24], including those who based on the above IFE-PIC algorithm[25]. Some of them do not update the wall surface, only calculate the corrosion quantity by the sputter parameters obtained in previous process[6,21,25].These results are just a rough estimation of the device's lifetime. Others studies terminate the program, adjust the object boundary and remesh the model for the new phase[22]. The latter one is more relative practical but too much manually performed and time-consuming.

This paper presents an improved two-dimensional axisymmetric hybrid IFE-PIC algorithm to solve moving interface problem without remeshing operation. It can more really present the characteristics of the particle's motion and wall erosion. Some work have been carried out to improve the IFE and PIC to realize this arithmetic. An important approach is inducted into this algorithm to describe the whole evolution process of the corrosion surface. It is based on the Huygens' wavelet construction approach which is introduced by Katardjiev et al [26-29].This approach performs well capability to handle various surface evolution problems quickly and accurately. Recently, this approach is even applied to illustrate the evolution of Hall thruster channel wall corners [30-32]. All the detailed descriptions are given in section 2.Section 3 gives a sequential algorithm of this moving boundary IFE-PIC method. Section 4presents a numerical and a practical examples and discusses the simulation results. Section 5provides a summary and conclusions.

 ISSN 2572-4975 (Print), 2572-4991 (Online)

2 Algorithm

2.1 IFE-PIC model

You can use sub-sections until the third order. Following is the example. In an electrostatic PIC simulation, the whole electric field is defined by the Poisson's equation[16,17,33]:

$$-\nabla \cdot (\varepsilon \nabla \Phi) = \nabla \cdot \mathbf{E} = e(n_i - n_e) \tag{1}$$

with boundary condition:

$$\Phi\big|_{\partial\Omega_D} = g_D \tag{2}$$

$$\varepsilon \frac{\partial \Phi}{\partial n}\Big|_{\partial\Omega_N} = g_N \tag{3}$$

where n_i is the ion density, ε is the permittivity, Φ is the electric potential, Ω_D and Ω_N are the boundary surface where Drichilet and Neumann boundary conditions apply, respectively. Additionally, the jump conditions across the interface the boundary surface where Drichilet and Neumann boundary conditions apply, respectively. Additionally, the jump conditions across the interface T:

$$[\Phi]_T = 0 \tag{4}$$

$$\left[\varepsilon \frac{\partial \Phi}{\partial n}\right]_T = 0 \tag{5}$$

are essential for a interface problem. The dielectric constant ε has different value inside(ε^+)and outside (ε^-) of the object interface.

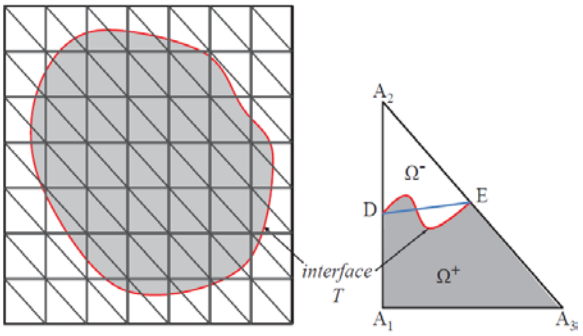

Fig. 1. Sketches of IFE mesh and the interface element.

The structured mesh is the key characteristic of the IFE algorithm and it is also the foundation for the Huygens construction. The whole solution domain is firstly meshed into uniform squares, and further partitioned into two triangles. Since the mesh of IFE is independent of the interfaces, some of the elements will cut by the interfaces. Those elements are called interface elements, and each of them must have two intersections, as shown in Fig.1. The information as vertex location, vertex type, element type are gathered for each element. But for the interface elements, the intersections (*D* and *E*), element properties for each sub-element are also need to be recorded.

The structured mesh is the key characteristic of the IFE algorithm and it is also the foundation for the Huygens construction. Hence, the following gives a detailed description of the partition process.

For a typical interface triangular element Γ with three vertices A_1, A_2 and A_3, as shown in Fig.1, it is divided into two sub-elements: $\Gamma^+ = T \cap \Omega^+$ and $\Gamma^- = T \cap \Omega^-$ by the interface T. With this natural partition of T, the three piece wise linear local nodal basis functions can be expressed as [33,34]:

$$\psi_i = \begin{cases} \psi_i^+ = a_1 x + b_1 x + c_1 \\ \psi_i^- = a_2 x + b_2 x + c_2 \end{cases} \quad (i = 1,2,3) \tag{6}$$

With following constraints:

1. Nodal values specification:

$$\psi_i(A_j) = \begin{cases} 1, i = j \\ 0, i \neq j \end{cases} \quad (i, j = 1,2,3)$$

2. The continuity across the interface inside the triangular element $\Gamma_T = T \cap \Gamma$:

$$\psi_i^+(P) = \psi_i^-(P) \quad i = 1,2,3$$

where P is the intersections D and E.

3. The flux continuity across $\tilde{\Gamma}_T$:

$$\int_{\tilde{\Gamma}_T} (\varepsilon^+ \frac{\partial \Psi_i^+}{\partial \mathbf{n}} - \varepsilon^- \frac{\partial \Psi_i^-}{\partial \mathbf{n}}) ds = 0 \quad i = 1,2,3$$

$\tilde{\Gamma}_T$ is the surface determined by the points D and E, $\mathbf{n}$ is the normal of $\tilde{\Gamma}_T$.

The right hand of the equation 1 is obtained by gathering all particle charge in each elements. All particle trajectories are governed by Newton's second law:

$$\frac{d}{dt}(m\mathbf{v}) = \mathbf{F} = q\mathbf{E}, \mathbf{v} = \frac{d\mathbf{x}}{dt} \tag{7}$$

where m, $\mathbf{v}$, $\mathbf{x}$ and q are the mass, velocity, position and charge of the ions, $\mathbf{E}$ and $\mathbf{F}$ are the electric field intensity and force, dt is the time step. PIC method use macro particle [13] which present a lot of real particles to simulate the plasma flow. The typical computing procedure of a PIC algorithm is:

1. Inject constant number of macro particles with the given velocities.

2. Push particles by the current electric field with equation 7.

3. Weight the particle charges to the neighbor four mesh nodes by particle positions, as shown in Fig.2. The Verboncoeur weighting factor[35] is used for the radial component in order to take into account the cylindrical metrics, while a linear weighting is used for the azimuthal component: The contribution of the particle P to the charge density at node (i, j) is calculated from.

$$q(i, j) = q_p \frac{V_{(X_{(i+1,j+1)}, X_p)}}{V_{(X_{(i,j)}, X_{(i+1,j+1)})}}$$

where q_p and X_P are the charge and location of the particle P, $X_{(i,j)}$is the location of node (i, j) and $V_{1,2}$ is the rectangular area defined by nodes 1 and 2.

 ISSN 2572-4975 (Print), 2572-4991 (Online)

4. Solve the electrostatic field by equation 1 with the obtained space charge density.

5. Weight the electric force from mesh nodes to particle locations, the approach is similar to the step 3. The electric force will used to update the velocities and positions of each particles.

2.2 Dynamic boundary algorithm

Many kind of approaches can be used to predicate the surface evolution: the characteristic method [26, 36], the level set method [37-39] and the wavelet method [26-32]. In this study,the wavelet method, which is based on the Huygens principle, is used to describe the process of surface evolution. This wavelet method considers the evolution surface as a wave front and each point on this surface as an independent wavelet source. The wave propagation rate is the erosion rate, the new evolved surface is the tangent envelope surface of all the wave fronts of the wavelets.

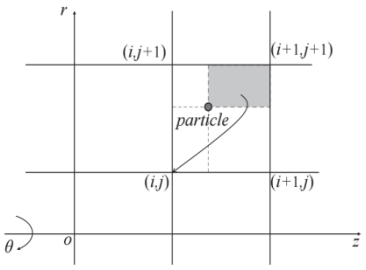

Fig. 2. Deposition of particle charge in a two-dimensional axisymmetric domain.

Generally, the surface evolution can be described by the equation:

$$S(x,y,z,t)=0 \tag{8}$$

If S is differentiable everywhere in the defined interval, it then satisfies the partially equation:

$$\frac{\partial S}{\partial t}+\boldsymbol{c}\cdot\nabla S=0 \tag{9}$$

where $\boldsymbol{c}=R\cdot\boldsymbol{n}$ is the normal velocity, R is the evolution rate and $\boldsymbol{n}$ is the normal vector of the given surface. The position of the interface S at all time can be described by a first order nonlinear hyperbolic partial differential equation (also known as a Hamilton-Jacobi equation):

$$S(t)+R\sqrt{S_x^2+S_y^2+S_z^2}=0 \tag{10}$$

Katardjiev gives the solutions of this equation in the vector form:

$$\boldsymbol{V}=\boldsymbol{c}+(\boldsymbol{n}\times\nabla_n R)=0 \tag{11}$$

$$\frac{d\boldsymbol{n}}{dt}=(\boldsymbol{n}\times\nabla_r R)\times\boldsymbol{n} \tag{12}$$

where $\nabla_n = (\frac{\partial}{\partial n_x}, \frac{\partial}{\partial n_y}, \frac{\partial}{\partial n_z})$, $\nabla_r = (\frac{\partial}{\partial x}, \frac{\partial}{\partial y}, \frac{\partial}{\partial z})$. In a two-dimensional x-y Cartesian coordinate system, the two components of the evolution velocities can be written as:

$$V_x = \frac{dx}{dt} = \frac{\partial R}{\partial \theta_i} \cos^2 \theta_i \tag{13}$$

$$V_y = \frac{dy}{dt} = R - \frac{\partial R}{\partial \theta_i} \sin\theta_i \cos\theta_i \tag{14}$$

where, θ= arccos($\boldsymbol{c}R$).

In case it is a two-dimensional erosion model and the ions incident along the -y direction, the value of erosion rate is usually given by:

$$R = \frac{J_i Y(E_i, \theta_i)\cos\theta}{N_{sub}} \tag{15}$$

where, J_i is the incident flux density, N_{sub} is the atomic density of the substrate material, Y (E_i, θ_i) is the sputtering yield (atoms/ion) and E_i and θ_i are the energy and angle of the incident ions. The E_i and θ_i are independent influencing factors of the sputtering yield Y (E_i, θ_i), thus the sputtering yield Y (E_i, θ_i) can be expressed into :

$$Y(E_i, \theta_i) = Y(0) \cdot Y(\theta_i) \tag{16}$$

where, Y(0) is the product of the normal sputter yield and Y (θ_i) is the angular yield.

Then the characteristic velocity components of an arbitrary wavelet source take the following forms:

$$V_x = \frac{dx}{dt} = \kappa \frac{dY(\theta_i)}{d\theta_i} \cos^2 \theta_i \tag{17}$$

$$V_y = \frac{dy}{dt} = \kappa Y(\theta_i) - \frac{dY(\theta_i)}{d\theta_i} \sin\theta_i \cos\theta_i \tag{18}$$

where $\kappa = \frac{J_i Y(0)}{N_{sub}}$, the incident angle θ_i various from $-\pi/2$ to $\pi/2$. The sketch of the characteristic velocity component (CVCP) is shown in broken lines in Fig.3. And if the ions incident with an angle θ_i, the CVCP should rotate the corresponding angle as shown in solid line in Fig.3 as well.

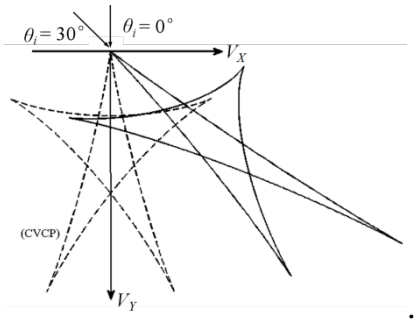

Fig. 3. The two dimensional characteristic component velocity plot (CVCP).

 ISSN 2572-4975 (Print), 2572-4991 (Online)

It has absolutely advantages to incorporate Huygens wavelet method with the above IFE-PIC algorithm. Because PIC method stores up all the incident information and IFE gives a sectional interface. Let take the evolution process of an arbitrary intersection O and the adjacent two interface sections for example, the working method of Huygens wavelet approach is stated as follows. As shown in Fig.4, the two sections OD and OE move to new positionsO_1D_1 and O_2E_1 at their own propagation rates. Their rates are given by the equation 1with the mean number $N_i$and energies E_i, but the original angle θ_i of their own. Then the intersection O evolved as a wave source under the mean incident condition of both sides. The CVCP will have two points of tangency O_3 and O_4 with the segments O_1D_1 and O_2E_1. TheO_3D_1, O_4E_1 and a part O_3O_4 of the CVCP form the final curve. The complete evolution surface will seen as obtained after all the intersections are reconstructed.

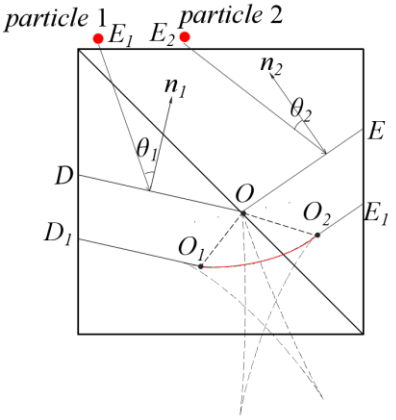

Fig. 4. Schematic representation of the construction by Huygens wavelet method

3 Sequential algorithm of dynamic boundary IFE-PIC

In this section, we give out a brief demonstration of the dynamic boundary IFE-PIC. The responding flowchart is also given by Fig.5.

STEP 1: Define the geometry of the immersed objects and the boundary conditions of the simulation domain. Set up a Cartesian rectangular mesh and then partition each cell into the triangle submesh by its diagonal line. Do all preparation work for the PIC.

STEP 2: Consider the Poisson's equation of the electrostatic problem as described in Eq.1. Define the properties of all the elements and nodes. The nodes have two types: inside the object(Ω^+) with ε^+ and outside the object(Ω^-) with ε^-. Beside these two types, the elements have another type-interface elements($\Gamma^+ \cap \Gamma^-$). Store up the information of the interfaces elements and intersections . Do all preparation work for the IFE.

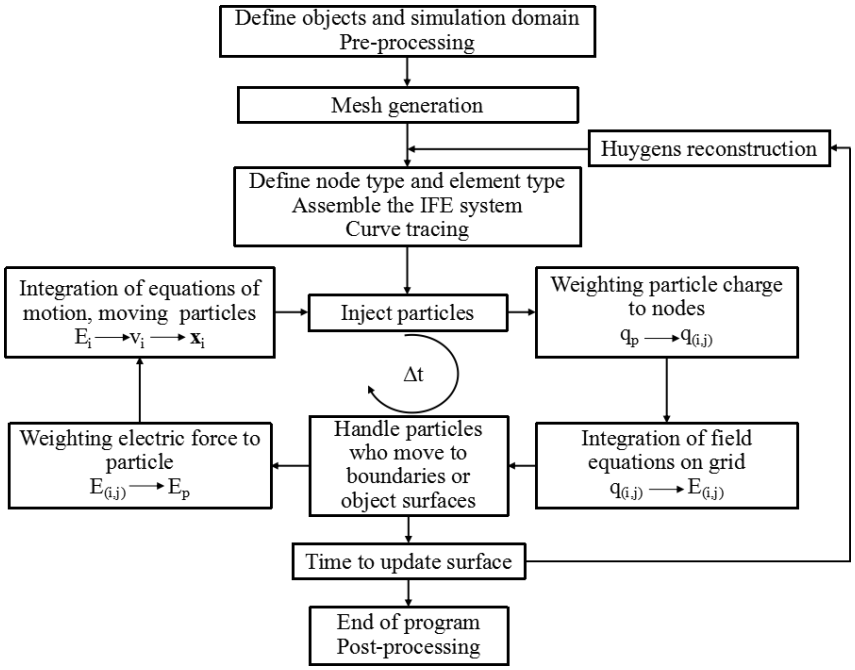

Fig. 5. Flowchart of the dynamic boundary IFE-PIC method.

STEP 3: Tracing out the surface curves which will be eroded latter. The curves can be obtained through an input ascii file or by defining the algebraic equations when the surface is a rule curve. But here we consider the more usual case, the irregular surface curve. It is worthy of special attention that we have obtain and store all the intersection topologies in a index array Tint in IFE. As shown in Fig.6, for a closed curve, we give an arbitrary intersection1 of this object and then the other intersection 2 is determined within the same elements.This element is marked been used and deleted from the Tint. The neighbor element must be accessed by searching in the new array Tint for the intersection 2, thus along with it is the certitude of the next node 3. Repeat these processes until the intersection 1 is found out again.Now all interface elements should have been searched for one time and the surface curve is obtained. While for an unclosed curve, we should offer some invariants to determine the surface topology, such as the two fixed endpoints of this curve. When doing curve tracing, we first start from one endpoint and do the same processes as tracing for a closed curve. The complete curve message will be obtained until the other endpoint is found out.

STEP 4: Inject and move particles, then estimate their locations. Keep a record of the ions whose incident on the eroded surface.

STEP 5: If it is the time step to update the evolution surface, do the Huygens construction and get the new geometry of the wall. Redefine the interface elements and intersection according to the new wall. Update the properties of all the elements and nodes. Redo the preparation work for IFE. Otherwise, if the surface not evolved, go to the step 6.

STEP 6: Tracing out the new surface curves by the new interface elements and intersections.

STEP 7: Count up the charge densities and solve the Poisson equation. If it is not the end of the program, return to step4, or terminate this simulation.

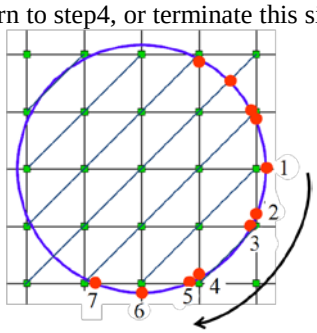

Fig. 6.A sketch of the method for the curve tracing.

4 Numerical examples

4.1 Numerical model for dynamic boundary immersed element

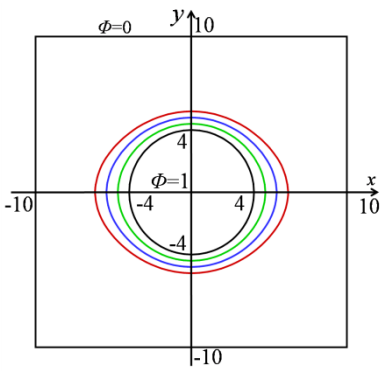

Fig. 7. The curve plots of each evolution phase.

In this section, the evolution process of a circle is simulated to show the feasibility and accuracy of the dynamic boundary IFE method. It is a 2-D simulation model, the square domain Ω_s= [−10, 10]× [−10, 10] and the circle with radius r = 4 whose center locates at the origin of the coordinate is shown in Fig.7. The potential inside the circle is fixed at Φ= 1, while the square domain boundary is set to be Dirichlet boundary condition, Φ= 0. The mesh size is set to be h = 1.0 and the evolution rate R is constant value by a given elliptic expression:

$$R = \frac{b}{\sqrt{1 - a \cdot \cos^2 \theta_i}} \tag{19}$$

where $a = 0.7$, $b = 0.4$ and $\cos^2\theta_i = \frac{x^2}{x^2 + y^2}$. X and y are the coordinate values of the local point. Fig.8a shows the original analytical solution of this model. Fig.8b, 8c, 8d are the simulation results after evolved one step, two steps and three steps.

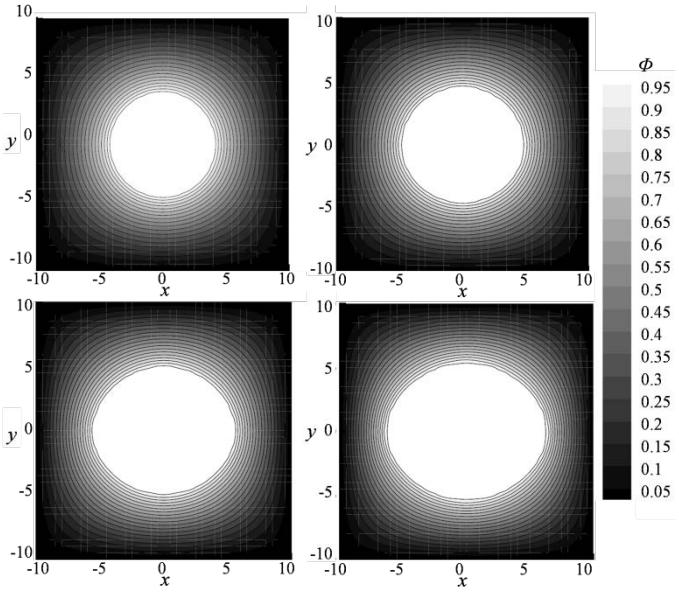

Fig. 8. The potential results of a given evolution rate circle.

4.2 Practical model of ion thruster accelerator grid erosion

In this section, we present a numerical example to demonstrate the performance of the dynamic boundary IFE-PIC method developed in the previous sections for simulating the grid erosion problem. This 2-D symmetric model is based on the ion optic thruster with hypothetical single aperture locate on the axis. The reference variables for normalization are list in Table1. The dimensions and throttling condition[40] of this simulation are given in Table 2. The sedates are based on the NASA's Evolutionary Xenon Thruster (NEXT) system. The layout of ion optics for this simulation ranges from the upstream discharge plasma to the downstream neutralization plasma, as shown in Fig.9.

The hybrid IFE-PIC method is a simplified method to solve plasma problem, in which the electrons follow the Boltzmann's distribution:

$$n_e = n_{eo} \exp\left(\frac{e(\Phi - \Phi_0)}{kT_{eo}}\right) \tag{20}$$

where Φ_o, n_{eo} and T_{eo} are, respectively, the potential, electron density and temperature for reference, n_e is the local density of electron. The beam ions are still modeled as particles and those who move to the symmetry axis are reflected, whereas those move to the other sides or objects are absorbed. The number N_i, energies E_i and angles θ_i of those particles who collide with an object is carefully recorded and accumulated by

 ISSN 2572-4975 (Print), 2572-4991 (Online)

the unit of line segments of the object boundary, as shown in Fig.4. These data will later be used to calculate the erosion rate of the evolution surface.

Table 1. Reference parameters for the normalization

Variable name	Reference
mass	$m_i = 2.18 \times 10^{-25}$kg
charge	$q_e = 1.602 \times 10^{-19}$C
density	$n_{ref} = 1.0 \times 10^{17}$m^{-3}
length	$\lambda_D = \sqrt{\varepsilon k T_{ref} / ne^2} = 5.25531 \times 10^{-5}$m
energy	$T_{ref} = 5eV$
velocity	$v_{ref} = \sqrt{kT_{ref} / m_i} = 1.917 \times 10^3$m/s
time	$t_{ref} = \lambda_D / v_{ref} = 2.741 \times 10^{-8}$s

Table 2. Dimensions and throttling condition[40]

	Nominal value	Normalized value
screen hole diameter, d_s	0.002305 m	43.85
screen grid thickness,t_s	0.000461 m	9
acceleration grid diameter, d_a	0.001396 m	26.56
acceleration grid thickness, t_a	0.001016 m	19
screen to acceleration grid gap, l_g	0.000788 m	15
net accelerating voltage, Φ_n	1800 V	360
screen grid voltage, Φ_s	1780 V	354
acceleration grid voltage, Φ_a	-210 V	-42

For the aim of grid erosion, we consider a extreme operating condition which represents cross-over condition with only one aperture. The reference parameters of the electron density temperature, density and potential for Boltzmann's distribution of upstream plasma are T_{eup}=5eV, n_{eup}= $0.05\times10^{17}m^{-3}$ and Φ_{up}= Φ_n, while these parameters of downstream plasma are T_{edown}= 1.5eV, n_{edown}= $0.005\times10^{17}m^{-3}$ and Φ_{up}= 0. On the other wise, the ions are inject into the domain from the left side with the density n_{io}= $0.05\times10^{17}m^{-3}$ and temperature is about 300K. This temperature is equal to the temperature of discharge chamber wall. The whole simulation domain is taken to be 220×26, with the cell size $\Delta \approx \lambda_D$. The screen grid locates at z=80 and the other sets can be found in Table 2 and Fig.9. All simulation sides are fulfill the Neumann boundary conditions except the left side is set to be Dirichlet boundary conditions. Those particles move to the upper or down side will be reflected, whereas those move

to the other sides or objects are absorbed. No collision among particles is considered in this simulation. The time step is set to be 0.1, above than 6300 particles is emitted into this domain per step and the whole number reaches above 27 million at t=2000 (20000 steps)before the data statistics for erosion. Until t=2000, the simulation for cross-over condition is considered into a stable state and then the accelerator grid surface starts evolve. The number N_i, energies E_i and angles θ_i of those particles who collide with a object is carefully recorded and accumulated by the unit of line segments of the object boundary every 2000 steps after t=2000. At the end of each 2000 steps, the accelerator grid surface evolves and a new surface is constructed.

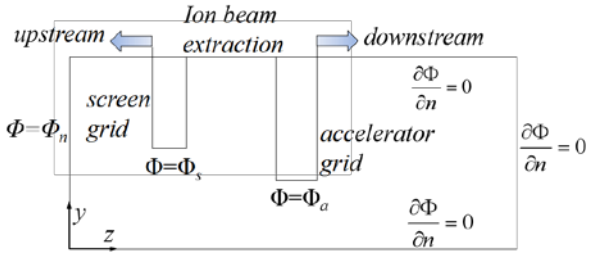

Fig. 9.A sketch of the domain for the grid erosion problem.

In this simulation, the product of the normal sputter yield $Y(0)$ is given by [23]:

$$Y(0) = -7.297\times10^{-7}E_i^2 + 2.515\times10^{-3}E_i - 0.1866 \quad (21)$$

$$Y(0) = -5.559\times10^{-8}E_i^2 + 1.090\times10^{-3}E_i + 0.4778 \quad (22)$$

while the angular yield $Y(\theta_i)$ is based on the Yamamura empirical formula [41, 42]:

$$Y(\theta_i) = x^f\exp[-\Sigma(x-1)] \quad (23)$$

where $x = 1/\cos\theta_i$, Σ and f satisfy: $\Sigma/f = \cos\theta_{opt}$. $\theta_{opt}$is the optimal angle of xenon on molybdenum,its value is usually taken as 47 degrees [23, 43]. As was mentioned above, the number N_i, energies and angles of incident ions have been recorded down on each interface segments.Averaging the energies and angles by the incident number, we get the mean sputtering energy E_i and angle θ_i. Then the erosion rate R is calculated by the equation 1 with the incident energy E_i and angles θ_i and the number N_i.

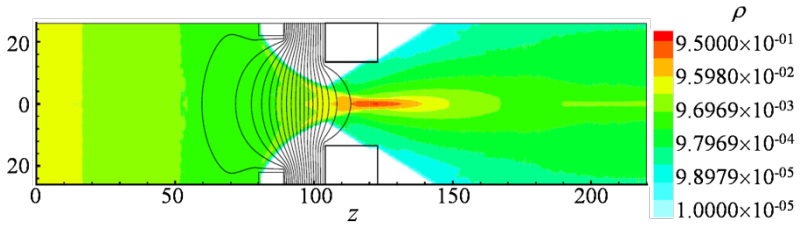

Fig. 10. The potential and particle density of the steady cross-over condition without grid erosion.

Fig.10 is the beam let ion density contours and selected potential contour lines for the cross-over condition. The simulation data is mirrored about the z plane to illustrate the whole beam let flow through a single aperture. Obviously, the accelerate grid is drastic collided by ions. Fig.11(a) gives the descriptions of surface curve motion at each evolution phase. From the first evolution step of the simulation results and the

 ISSN 2572-4975 (Print), 2572-4991 (Online)

benchmark results, it is easy to find that the maximum erosion depth locate near the beginning of the incident ion beam when the evolution starts. This location move behind as the surface further evolved from the late revolution simulation results. At the end of evolution, the accelerator grid corner is gradually eroded away and the evolution surface is parallel to the ion beam divergence angle. Thus,if the grid surface is stable, the ultima surface will keep the parabolic profile, as shown in Fig.11(b). Fig.12a and Fig.12b are the drawing of partial enlargement near the accelerator grid. Obviously, the accelerator grid is sputtered by the high energy ion beam let as shown in Fig.12a. In Fig.12b, the right corner of the accelerator grid is almost eroded away. This result is obvious more real and credible.

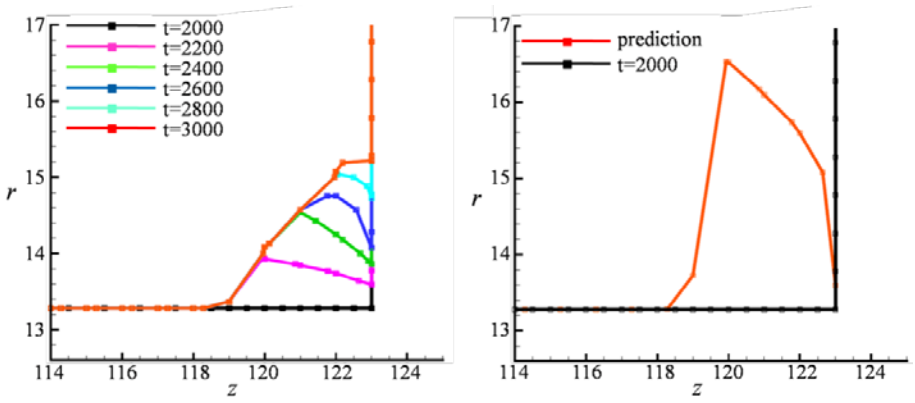

(a) Curves by dynamic boundary IFE-PIC(b) Curves by predict erosion depth

Fig. 11. Surface curves of the accelerator grid.

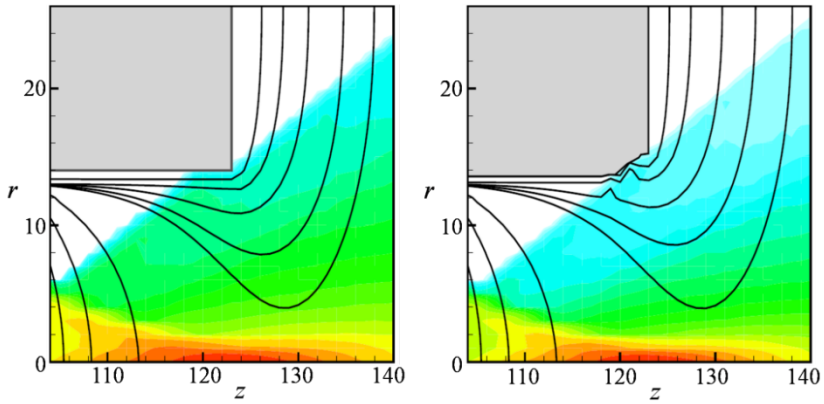

(a) *t*=2000 (b) *t*=3000

Fig. 12. The local distribution of potential and particle density.

5 Conclusions

This paper presents a moving boundary IFE-PIC method for modeling plasma-wall Interaction. The IFE establishes a Cartesian mesh and gives the information of intersections for tracing the evolution surface. The Huygens wavelet method is imported into the IFE-PIC algorithm to handle the evolution process of interface curve. This moving boundary IFE-PIC method fully use and develop the advantage of the IFE algorithm. Additionally, the moving boundary IFE-PIC method allows us to obtain good approximations of surface evolution problems on Cartesian meshes, which is very important to many applications. The significations and practical values for this method are:

1. Do real and exact information capturing of the particle trajectories and the local electric field when the object boundary is sputtered and evolved.
2. Performs high automation and simple operation, boundary evolution inside executing program without intervene manually give the guarantee of continuity of the simulation.
3. Extend and improve the IFE-PIC algorithm.Two numerical examples, the evolution of a circle with given evolution rate and the erosion of ion thruster accelerator grid erosion, are given in the penultimate section. The results obtained confirm that this moving boundary IFE-PIC method provide viable and reliable computational tools for simulating plasma problem with moving interface. This method also shows great significance for improving plasma device design, predict their service life, and understand the failure modes

Acknowledgement

This work was financially supported by the University Distinguished Young Research Talent Training Program of Fujian Province under Grant No. JAT160835, and the Technology Project of Education Department of Fujian Province under Grant No. JAT160831.

References

1. G. Maderlechner R. Behrisch and B. M. U. Scherzer. The sputtering mechanism forlow-energy light ions. ***Applied Physics***, 18 (2014) 2547-2556.
2. M. Nakano. Sensitivity analysis of the effects of doubly charged ions on ion acceleration grid erosion. ***Transactions of The Japan Society for Aeronautical and Space Sciences***, 55 (2012) 364-372.
3. S. Deambrosis D. Dellasega E. Vassallo, R. Caniello and F.Ghezzi. Removing of mixed coatings by plasma discharges. ***Journal of Fusion Energy***, 32(6) (2013) 642-644.
4. G. Genta, ***Dynamics of Rotating Systems***, Springer Science+Business Media, Inc., New York, 2005.
5. M. Nakano. Doubly charged ion effect on life prediction accuracy of ion acceleration grid system. ***Vacuum***, 88 (2013) 70-74.

 ISSN 2572-4975 (Print), 2572-4991 (Online)

6. J. W. Emhoff and I. D. Boyd. Grid erosion modeling of the next ion thruster optics.***39th AIAA/ASME/SAE/ASEE Joint Propulsion Conference and Exhibit***, pages 03-4868. AIAA, July, 2003.
7. E. Hartmann M. Tartz and H. Neumann. Evolution of extraction grid erosion with operation time.***40th AIAA/ASME/SAE/ASEE Joint Propulsion Conference and Exhibit***,, pages 04-3787. AIAA, July, 2004.
8. Z. Zhen-peng J. Zhi-guo G. Zuo L. Chang, T. Hai-bin and L. Juan. Numerical simulation and dff measurement of ion thruster accelerator grid erosion depth. ***Journal of Aerospace-Power***, 23(3) (2008) 574-9.
9. J. R. Brophy and G. B. Ganapathi. Status of the dawn ion propulsion system. ***40thAIAA/ASME/SAE/ASEE Joint Propulsion Conference and Exhibit***, pages 04-3433. AIAA, July, 2004.
10. G. B. Ganapathi et al. J. R. Brophy, M. G. Marcucci. Implementation of the dawn ionpropulsion system. ***41st AIAA/ASME/SAE/ASEE Joint Propulsion Conference andExhibit***, pages 05-4071. AIAA, July, 2005.
11. V. Shutthanandan M. R. Nakles, J. Wang and Yanwen Zhang. Further investigation of low-energy ion sputtering in ion thrusters. ***40th AIAA/ASME/SAE/ASEE Joint Propulsion Conference and Exhibit***, pages 04-3789. AIAA, July,2004.
12. G. Mao A. Sun and J. Yang. Particle simulation of three-grid erc ion thruster optics and erosion prediction. ***Plasma Science and Technology***, 12(2) (2010) 240-247.
13. C. K. Birdsall and A. B. Langdon. ***Plasma Physics via Computer Simulation***. Institute of Physics Publishing, New York, 1991.
14. R. C. Rogers T. Lin, L. Yanping and L. M. Ryan. ***A rectangular immersed finite element method for interface problems***, in: P. Minev, Y. Lin, volume 7. Nova Science Publishers,Inc., 2001.
15. L. Yanping H. Xiaoming, T. Lin and Zhang Xu. Immersed finite element methods forparabolic equations with moving interface. ***Numerical Methods for Partial Differential Equations***, 29(2) (2013) 619-646.
16. J. Wang R. Kafafy and T. Lin. A hybrid grid immersed finite element particle-in-cell algorithm for modeling spacecraft-plasma interactions. ***IEEE Transactions on Plasma Science***, 34(5) (2006) 2114-2124.
17. R. Kafafy and J. Wang. A hybrid grid immersed finite element particle-in-cell algorithm for modeling space craftc plasma interactions. ***IEEE Trans. Plasma Sciences***, 34(5) (2006) 2114-2124,.
18. R. Kafafy J. Pierru J. Wang, Y. Cao and V. K. Decyk. Simulations of ion thruster plumec space craft interactions on parallel supercomputer. ***IEEE Trans. Plasma Sciences***,34(5) (2006) 2148-2158,.
19. T. Lin and J. Wang. The immersed finite element method for plasma particle simulation.***Proceedings of AIAA Aerospace Sciences Meeting.***, *2003*. AIAA, 2003-0842.
20. T. Lin and J. Wang. An immersed finite element electric field solver for ion optics modeling.***Proceedings of AIAA Joint Propulsion Conference***,*2002*.AIAA, 2002-4263.
21. V. J. Friedly D. Keefer Xiaohang Peng, W. M. Ruyten and Quan Zhang. Particle simulation of ion optics and grid erosion for two-grid and three-grid systems. ***Review of Scientific Instruments***, 65(5) (1994) 1770-1774.
22. M. Gamero-Castano and I. Katz. Estimation of hall thruster erosion using Hphall. ***29th International Electric Propulsion Conference, Princeton***, pages 303-312. IEPC, October, 2005.

23. J. E. Polk J. R. Brophy, I. Katz and J. R. Anderson. Numerical simulations of ion thruster accelerator grid erosion. ***38th AIAA/ASME/SAE/ASEE Joint Propulsion Conference and Exhibit***, pages 02-4261. AIAA, July, 2002.
24. M. Nakano and Y. Arakawa. Ion thruster lifetime estimation and modeling using computer simulation. ***26th International Electric Propulsion Conference***,pages 99-145. IEPC, October, 1999.
25. J. Brophy J. Wang, J. Polk and I. Katz. Three-dimensional particle simulations of ion optics plasma flow and grid erosion. ***Journal of Propulsion and Power***, 19(6) (2003) 1192-1199.
26. G. Carter I. V. Katardjiev and M. J. Nobes. The application of the Huygens principle to surface evolution in homogeneous, anisotropic and time-dependent systems. ***Journal of Physics D: Applied Physics***, 22(12) (1989) 1813-1824,.
27. M. J. Nobes I. V. Katardjiev, G. Carter and R. Smith. Precision modeling of the mask substrate evolution during ion etching. ***Journal of vacuum science and technology. A.Vacuum, surfaces, and films***, 6(4) (1988) 2443-2450.
28. I. V. Katardjiev. A kinematic model of surface evolution during growth and erosion:Numerical analysis. ***Journal of vacuum science and technology. A. Vacuum, surfaces, and films***, 7(6) (1989) 3222-3232.
29. G. Carter and M. J. Nobes. A kinematic model of surface evolution during growth and erosion: Numerical analysis. ***Journal of materials science letters***, 3(6) (1984) 523-527.
30. Yuquan Li and Daren Yu. Reconstruction of ionization density distribution in hall thruster channel from ion energy spectrum of plasma jet. ***Plasma Science and Technology***, 8 (2006) 666-669,.
31. Yuquan Li Daren Yu and Shenhua Song. Ion sputtering erosion of channel wall corner sin hall thrusters. ***Journal of Physics D: Applied Physics***, 39 (2006) 2205-2211.
32. Daren Yu and Yuquan Li. Volumetric erosion rate reduction of hall thruster channel wall during ion sputtering process. ***Journal of Physics D: Applied Physics***, 40 (2007) 2526-2532.
33. R. Kafafy. ***Immersed finite element Particle-In-Cell simulations of ion propulsion***. PhD thesis, Virginia Polytechnic Institute and State University, Blacksburg, Virginia, September 2005.
34. Xiaoming He Yucuan Chu, Yong Cao and Min Luo. Asymptotic boundary conditions with immersed finite elements for interface magneto static/electrostatic field problems with open boundary. ***Computer Physics Communications***, 182 (2011) 2331-2338.
35. J. P. Verboncoeur. Symmetric spline weighting for charge and current density in particle simulation. ***Journal of Computational Physics***, 174 (2001) 421-427.
36. A. I. Morozov and V. V. Savelyev. Fundamentals of stationary plasma thruster theory.***Reviews of Plasma Physics***, 21 (2001) 203-391.
37. D. Adalsteinsson and J. A. Sethian. A fast level set method for propagating interfaces.***Journal of Computational Physics***, 118 (1995) 269-277.
38. D. Adalsteinsson and J. A. Sethian. A unified level set approach to etching, deposition and lithography i: Algorithms and two-dimensional simulations. ***Journal of Computational Physics***, 120 (1995) 128-144,.
39. D. Adalsteinsson and J. A. Sethian. A unified level set approach to etching, deposition and lithography ii: Three-dimensional simulations. ***Journal of Computational Physics***,122 (1995) 348-366.
40. Y. Cao J. Wang and R. Kafafy. Numerical and experimental investigations of crossover ion impingement for subscale ion optics. ***Journal of Propulsion and Power***, 24(3) (2008) 562-570.

41. Y. Yamamura and H. Tawara. Energy dependence of ion-induced sputtering yields from monatomic solids at normal incidence. ***Atomic Data and Nuclear Tables***, 62(2) (1992) 149-253.
42. Y. Itikawa Y. Yamamura and N. Itoh. Angular dependence of sputtering yields of monatomic solids. ***Nagoya University Institute of Plasma Physics Report***, pages IPPJ-AM-26, 1983.
43. C. Farnell M. Butweiller A. P. Yalin, V. Surla and J. D. Williams. Sputtering studies of multi-component materials by weight loss and cavity ring-down spectroscopy. ***42nd AIAA/ASME/SAE/ASEE Joint Propulsion Conference and Exhibit***, pages 06-4338. AIAA, July, 2006.